The interaction of water and hydrogen with nickel surfaces
Shan, J.

Citation
Shan, J. (2009, November 11). *The interaction of water and hydrogen with nickel surfaces*. Retrieved from https://hdl.handle.net/1887/14365

Version:	Corrected Publisher's Version
License:	Licence agreement concerning inclusion of doctoral thesis in the Institutional Repository of the University of Leiden
Downloaded from:	https://hdl.handle.net/1887/14365

Note: To cite this publication please use the final published version (if applicable).

Chapter 4

Co-adsorption of water and hydrogen on Ni(111)

We have studied the surface coverage dependence of the co-adsorption of D and D_2O on the Ni(111) surface under UHV conditions. We use detailed temperature-programmed desorption studies and high resolution electron energy loss spectroscopy to show how pre-covering the surface with various amounts of D affects adsorption and desorption of D_2O. Our results show that the effects of co-adsorption are strongly dependent on D-coverage. In the deuterium pre-coverage range of 0 - 0.3 ML, adsorption of deuterium leaves a fraction of the available surface area bare for D_2O adsorption, which shows no significant changes compared to adsorption on the bare surface. Our data indicates phase segregation of hydrogen and water into islands. At low post-coverages, D_2O forms a two-phase system on the remaining bare surface that shows zero-order desorption kinetics. This two phase system likely consists of a two-dimensional (2D) solid phase of extended islands of hexamer rings and a 2D water gas phase. Increasing the water post-dose leads at first to 'freezing' of the 2D gas and is followed by formation of ordered, multilayered water islands in between the deuterium islands. For deuterium pre-coverages between 0.3 and 0.5 ML, our data may be interpreted that the water hexamer ring structure, $(D_2O)_6$, required for formation of an ordered multilayer, does not form anymore. Instead, more disordered linear and branched chains of water molecules grow in between the extended, hydrophobic deuterium islands. These deuterium islands have a D-atom density in agreement with a (2x2)-2D structure. The disordered water structures adsorbed in between form nucleation sites for growth of 3D water structures, which (partially) spill over the deuterium islands. Loss of regular lateral hydrogen bonding and weakened interaction with the substrate reduces the binding energy of water significantly in this regime and results in lowering of the desorption temperature. At deuterium pre-coverages greater than 0.5 ML, the saturated (2x2)-2D structure mixes with (1x1)-1D patches. The mixed structures are also hydrophobic. On such surfaces, submonolayer doses of water lead to formation of 3D water structures well before wetting the entire hydrogen-covered surface.

4.1 Introduction

Although the simultaneous interaction of water and hydrogen with various metal surfaces has been studied and reviewed [1-10], the nature of the interaction between these species remains poorly understood. Co-adsorption of hydrogen and water on nickel is of particular interest due to their simultaneous presence on the anode of alkaline fuel cells. Also in many industrial processes, such as steam reforming, hydrogen and water co-exist on the catalyst surface. Steam reforming is the chemical process, where at high temperatures (700-1100ºC) and pressure and in the presence of a metal-based catalyst (nickel), steam reacts with methane to yield CO and hydrogen.

For the Ni(111) surface, several studies have investigated adsorption of either H_2 [11-14] or H_2O [15-19]. Hydrogen is known to dissociately adsorb on Ni(111) with a low barrier to reaction, although large exposures are necessary to (nearly) complete saturation [11-14]. The saturation coverage is generally agreed to be 1.0 monolayer (ML) [12-14]. Hydrogen is known to adsorb into fcc three-fold hollow sites from both experimental and theoretical studies [12,14,20-22]. Around 0.25 ML, an IV-LEED study suggests formation of p(2x2) islands at ~150 K [12], whereas a more recent HREELS study claims formation of (2x2)-2H islands already at much lower coverages and at 100 K [23]. At 0.5 ML, a (2x2)-2H structure exists which develops with increasing coverage into the (1x1)-H saturated structure [14,23]. Adsorption using molecular beam techniques shows that there is no isotopic dependencies in reactivity [24]. Also for desorption, no isotopic dependencies have been observed [25]. Hydrogen mobility has been studied using laser-induced desorption and optical diffraction techniques [26]. The diffusion rate is found to be 10^{-15} cm^2/s at 65 K and 10^{-7} cm^2/s at 240 K. At ~ 100 K, the rate increases monotonically from 3 x 10^{-13} cm^2/s at $\theta \approx 0.02$ to 1.3 x 10^{-12} cm^2/s at $\theta \approx 0.5$.

Experimental studies find water adsorption to be non-dissociative [15]. DFT calculations agree that an H_2O molecule preferentially binds on-top and experiences a large barrier to dissociation into H + OH, although calculated binding energies vary significantly [27,28]. A temperature-programmed desorption (TPD) spectrum of water from Ni(111) shows a feature near 170 K that saturates whereas a feature originating around 155 K does not saturate with increasing exposure. The latter shows zero-order desorption

characteristics. The 170 K feature is attributed to (sub)monolayer desorption, whereas the 155 K feature is believed to be due to multilayer desorption [15-19]. Previous investigations of the structure of water at (sub)monolayer coverages reported a $(\sqrt{3}\times\sqrt{3})R30^o$ pattern at $\theta\sim1$ [16]. However, Gallagher *et al.* recently observed a labile $(2\sqrt{7}\times2\sqrt{7})R19^o$ structure using low-current LEED for a single water layer grown at 135 K. This structure was affected by prolonged exposure to the electron beam resulting in increased intensity near the $\sqrt{3}$ positions [15]. A second layer of water was reported to wet the first layer, but destroyed the $(2\sqrt{7}\times2\sqrt{7})R19^o$ structure. Only thicker layers formed an incommensurate ice structure, closely oriented to the Ni(111) surface. Recently, Nakamura *et al.* used infrared reflection absorption spectroscopy to study water adsorption on Ni(111) and suggested that hexamer water clusters with a ring-like shape dominate on the Ni(111) surface at wide (sub)monolayer water coverages at 20 K [29].

Although we are not aware of any UHV co-adsorption studies of H_2 and H_2O on Ni(111) to date, co-adsorption on Pt(111) has been studied and provides a reference for $H_2O/H/Ni(111)$. An early co-adsorption study employing high resolution electron energy loss spectroscopy (HREELS) claimed formation of H_3O^+ (or hydrated forms of the hydronium ion) under UHV conditions on Pt(111) [3]. Such H_3O^+ formation was also reported on other Pt surfaces [7,8]. For adsorption and desorption of a co-adsorbed layer, a survey of the literature up to recent years indicates several inconsistencies. For example, for Pt(111) co-adsorption has been described to results in "strong changes" in TPD spectra [2] and was found to have "little if any effect" [3]. Although these conflicting observations had both been made before [4,5], results from a recent study by Petrik and Kimmel [9] provide a tentative explanation for the older claims. In a study that focused on electron-stimulated desorption and reactions occurring in water adsorbed to Pt(111), they also investigated the influence of adsorbing deuterium prior to dosing ~2 ML D_2O. They find that, at low coverages, D atoms stabilize D_2O. This is indicated by the appearance of a separate TPD peak at higher desorption temperature (~175 K) at the expense of the ~168 K desorption feature from the water monolayer interacting with the bare Pt(111) surface. However, at a D-coverage of ~0.25 ML (assuming a saturation coverage for deuterium of 1.0 ML), the same peak shifts back to below 170 K and reduces in size. Apparently, changes in

desorption features on Pt(111) are strongly dependent on deuterium pre-coverage and, at different pre-coverages, TPD spectra can appear both different and similar to spectra taken for water desorbing from the bare metal.

Recently, we have initiated a combined TPD-HREELS study to elucidate how adsorbed hydrogen affects the metal-water interaction on Ni(111) [30]. For the hydrogen-saturated surface, we have suggested that atomically-bound hydrogen increases hydrophobicity and that multilayered water islands form at submonolayer coverages. Using isotopic labeling we have identified various vibrations and showed that there are no isotopic effects in adsorption or desorption. We also found no evidence for isotope exchange between atomically-bound hydrogen and deuterated water nor did we find evidence for formation of H_3O^+ or similar species. We attributed this to the H-Ni bond strength preventing such reactions. See Chapter 3 for detail description.

In the this chapter, we use detailed TPD studies in combination with HREELS to investigate how much smaller amounts of pre-adsorbed hydrogen affect adsorption of water at (sub)monolayer coverages on Ni(111). Since no isotopic effects have been reported in adsorption or desorption for both hydrogen and water, we use D_2 and D_2O in our studies and expect our results and conclusions to hold generally for hydrogen-water co-adsorption on Ni(111). After presenting our data, we discuss and compare our results in combination with conclusions from previous studies. Our analysis allows us to suggest in detail how pre-adsorbed hydrogen affects the bonding between water molecules on Ni(111) and what causes differences observed between Pt(111) and Ni(111) for this system.

4.2 Experiment

Experiments are performed in an UHV apparatus. This apparatus consists of two chambers, which are separated by a gate valve. The top level is equipped with an ion sputter gun, an atomic hydrogen source, a stainless steel leak valve, a home-built capillary array doser [31], and a quadrupole mass spectrometer (Balzers QMS 422) used for TPD measurements and residual gas analysis. The lower level is equipped with an upgraded ELS22 high resolution electron energy loss spectrometer and a double-CMA Auger Electron spectrometer (Staib Instruments). The base pressure of the system is less than 1×10^{-10} mbar.

The Ni(111) single crystal is cut and polished to less than 0.1° of the low Miller-index plane (Surface Preparation Laboratories, Zaandam, the Netherlands). It can be heated to 1200 K by electron bombardment and cooled to 85 K. The sample temperature is measured by a chromel-alumel thermocouple spot-welded to the edge of the crystal. Sample preparation and verification of cleanliness were described in detail in chapter 3 or Ref. 30. D_2O (99.96% isotopic purity, Aldrich Chemical company) is cleaned by repeated freeze-pump-thaw cycles after which helium (Messer, 99.999%) is introduced to the glass container to a total pressure of approximately 1 bar. When dosing water, monitoring the helium partial pressure in our vacuum apparatus allows for increased dosing accuracy.

After cleaning, the sample is kept at 85 K while dosing D_2 (Linde, 99.9%) through a stainless steel leak valve, followed by dosing D_2O with the sample placed 15 mm in front of the capillary array doser. The deuterium coverage, θ_D, is estimated from integrating the TPD feature in separate experiments in which only D_2 is introduced. The latter is required since dosing water is accompanied by dosing helium, which lingers in the vacuum system and distorts the baseline of the TPD traces for m/z 4 (4, M − D_2). The TPD integral of D_2 is converted to an absolute coverage using a separately determined calibration curve based on D_2 doses ranging from 1×10^{-6} to $20,000 \times 10^{-6}$ mbar*s. HREEL spectra were recorded at 5 to 9 meV resolution (FWHM) with typical 1×10^4 cps for the scattered elastic peak.

All TPD measurements were performed with a heating rate of 1.0 K/s. Desorption of water from a single crystal at this rate may result in complex changes in the baseline due to non-equilibrated conditions between vacuum and chamber walls during the experiment. In particular, we notice a pump tail in TPD spectra that seems related to the water coverage on the crystal. In order to accurately quantify the amount of adsorbed water that desorbs either in a single or two partially overlapping peaks, we have used various functional forms to fit desorption traces. We describe this here in detail since it is of some consequence to the analysis of our data and we find such discussion lacking in the literature for water desorption.

Water desorption from metal surfaces is often described in terms of mono- and multilayer desorption as indicated by two separate desorption peaks and in terms of zero- and first-order desorption kinetics. Initially, we used two Gaussian profiles to fit the low

and high temperature peaks also observed in our TPD traces, although neither zero- or first-order desorption kinetics result in truly Gaussian peak shapes. The differential equations describing such desorption can not be solved without assumptions or simplifications [32]. Therefore, we used more elaborate deconvolution functions to improve the fitting procedure. In particular, we fit each main peak with a function that combines a distorted Gaussian line shape with an exponential decay to account for the pump tail. The distorted Gaussian line shape is a multiplication of an inverted tangent hyperbolic with a Gaussian profile, both centered at the same peak value, T_p. The pump tail consists of an exponential decay multiplied by a regular tangent hyperbolic, centered at the same peak value, T_p. Enforcing the same value ensures that the pump tail has no variable delay relative to the original desorption from the single crystal. The tangent hyperbolic in the pump tail contribution accounts for the rate at which desorption from chamber walls is 'turned on'.

Figure 4.1 shows the best fitting results for a single experiment where we dosed 0.05 ML D followed by approximately 0.8 ML D_2O. The inset in figure 4.1a shows the raw data for a large temperature regime, whereas the figure 4.1a and 4.1b zoom in on the relevant temperature regime. For figure 4.1a, we used the elaborate fitting procedure. It shows the four contributions for the two main peaks observed in the spectrum as dotted lines (LT, LTP, HT, and HTP). The raw data is shown as a dashed line and the total fit is shown as a solid line. To reduce uncertainty in this fitting procedure, the ratio of peak heights of the low temperature peak (LT) with its pump tail (LTP) was fixed after determining this ratio for the more intense high temperature peak (HT, HTP). Also, the decay rate of the pump tail was determined for the high temperature peak and fixed accordingly for the low temperature peak in every experiment. Inspection of figure 4.1a shows that this procedure accurately reproduces the experimental trace. We also observe that the pump tail of the low temperature peak around 158 K completely overlaps with the main desorption trace of the high temperatures peak at 170 K. Although the example shown here results in fairly unambiguous decomposition, we note that the ambiguity increases when the low and high temperature peaks are closer in size and/or peak desorption temperature. Figure 4.1b shows the fit using partially overlapping Gaussians. The fit is obviously less accurate. However, when converting the integrated peaks to absolute coverages, where the reference for 1 ML

equals the maximum size of the decomposed high temperature peak, the simple fitting procedure yields the same results as the more elaborate fitting procedure within 10%. This is likely due to the proportionality of the desorption peak and its pump tail. Since the differences are small, we use the simple fitting procedure throughout this chapter to analyze TPD traces and determine absolute coverages, except when otherwise stated.
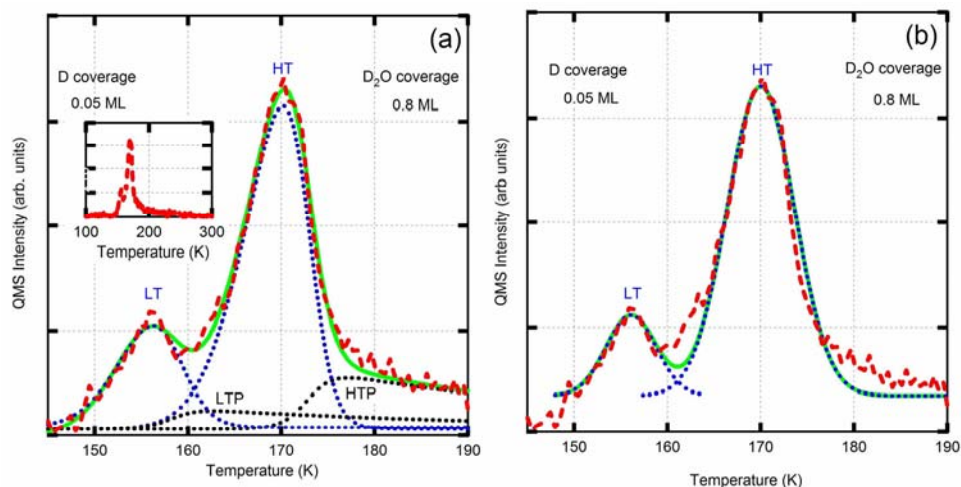

Figure 4.1 The fitting of D_2O TPD spectra from 0.8 ML deposited on 0.05 ML D pre-covered Ni(111) at 85 K. (a) Using the elaborate fitting procedure. (b) Using the simple fitting procedure with two Gaussian profiles. The inset shows the same TPD trace with temperature range from 100 K to 300 K. See text for abbreviations.

4.3 Results

Figure 4.2 displays six sets of TPD spectra of D_2O desorbing from various pre-coverages of deuterium on Ni(111). For $\theta_D = 0$ ML (Figure 4.2a), we only show water traces for $\theta_{D2O} \leq 1$ ML for clarity. Similar traces for $\theta_{D2O} > 1$ ML can be found in Chapter 3 and in reference [30]. For the bare Ni(111) surface, the D_2O desorption spectra show a single feature that initiates at ~166 K and shifts to ~170 K upon reaching saturation. Just before saturation, we observe a second feature at ~155 K. This low temperature feature has previously been shown not to reach saturation with increased dosing and shows zero-order desorption characteristics [15-19,30]. In figure 4.2a, this low temperature feature is just discernable as

a deviation from the baseline below 160 K for the 1 ML D_2O trace. It becomes more pronounced with larger dose or pre-covering with D (Figure 4.2b and 4.2c). We observe in our experiment that on the bare surface a 1.0 ML D_2O coverage consists of at most 0.15 and at least 0.85 ML of the low and high temperature features, respectively.
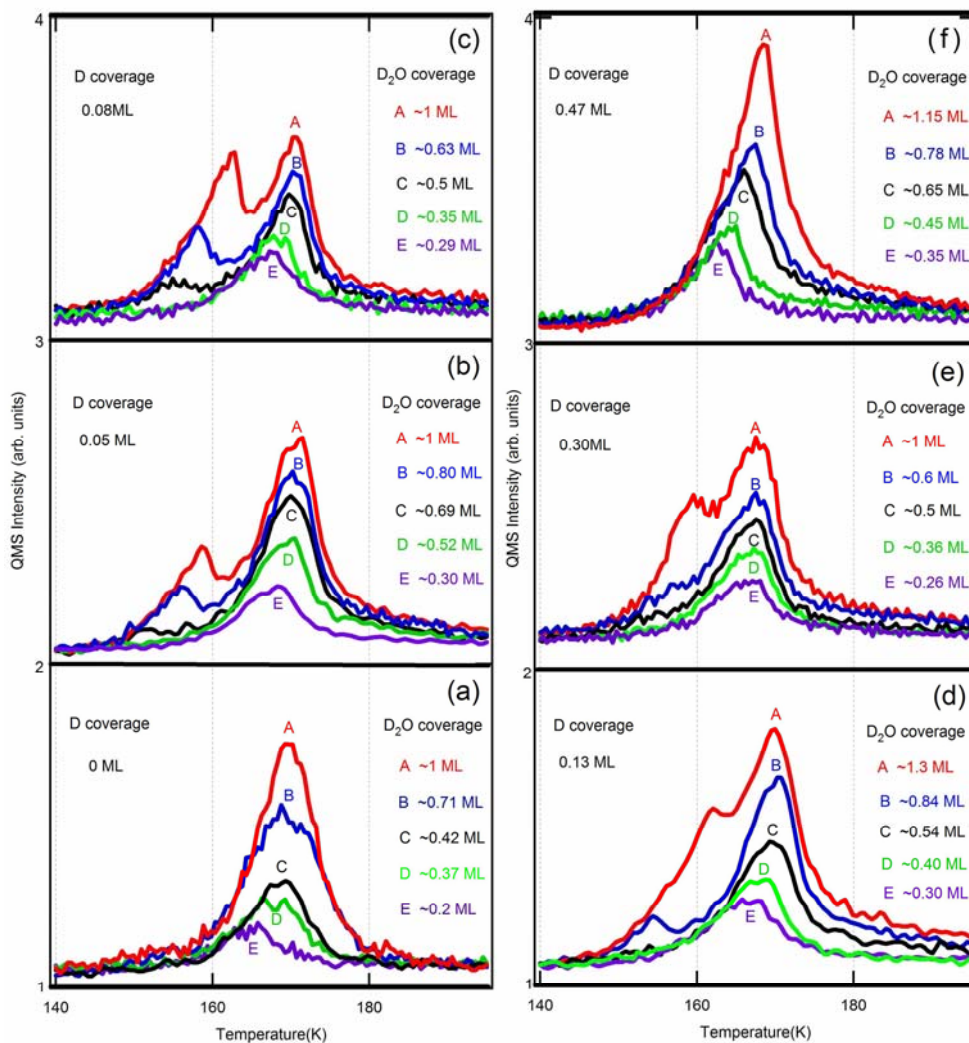

Figure 4.2 TPD of various amount of D_2O deposited on various D pre-coverages at 85 K.

Upon close inspection, figure 4.2 reveals detailed information on the influence of pre-adsorbed hydrogen on water adsorption. First, we notice that for $\theta_D = 0$ ML (Figure 4.2a)

traces C-E show typical characteristics of zero-order desorption kinetics: overlapping leading edges and desorption maxima shifting to higher temperature with increased dose [32]. However, for traces A and B the desorption maximum does not shift anymore and the leading edges do not coincide with the leading edge of trace C. This behavior is typical of first-order desorption kinetics. Upon inspection of previously published TPD spectra of water desorption from the bare Ni(111) surface we notice similar behavior, although it was not commented on by the authors [15-19]. In experiments using θ_D = 0.05, 0.08 ML and 0.13 ML (Figure 4.2b, 2c, and 2d) we observe the same behavior for water desorption. At low θ_{D2O}, characteristics of zero-order desorption kinetics are apparent for the high temperature desorption peak, whereas it switches to first-order desorption kinetics with increasing θ_{D2O}. In the same figures we also observe that the low temperature peak around 155 K develops at lower D_2O coverages with increasing D coverage. For θ_D = 0.05 ML, the low temperature peak appears near θ_{D2O} = 0.7 ML whereas for θ_D = 0.08 ML it is already observable around $\theta_{D2O} \approx 0.5$ ML. We note that, for $\theta_D \approx 0.13$ ML, its appearance seems delayed to $\theta_{D2O} \approx 0.8$ ML. This low temperature peak, starting at 155 K as a well defined peak and shifting upward with increased dose, shows typical zero-order desorption characteristics.

In contrast, at θ_D = 0.30 ML (Figure 4.2e), the lack of overlapping leading edges for the high temperature peak and the steadiness of the peak desorption temperature imply first-order desorption kinetics only. Whereas in figure 4.2a-d the peak temperature shifted to 170 K, it only reaches ~ 168 K here. Also, the low temperature peak grows in simultaneous with the high temperature peak in traces E, D, C and B. In figure 4.2b-d growth of the low and high temperature peaks are much more clearly separated.

For θ_D = 0.47 ML and $\theta_D \geq 0.35$ ML (Figure 4.2f), we observe only a single desorption feature with a peak temperature that smoothly shifts to higher values. Decomposition into a low and high temperature features is obviously not applicable here. Close inspection of the leading edges in figure 4.2f indicates that desorption resembles, but does not strictly follow, zero-order kinetics. For example, traces A and B share a leading edge only up to approximately half of the maximum desorption rate. The same is true for traces C and D.

Figure 4.3 shows additional water TPD spectra for $\theta_D = 0.47$ ML with water coverages ranging from 0.11 ML to 0.18 ML. Traces F, G and H, are off-set to show their first-order desorption characteristics more clearly. The leading edge of these traces deviates from the leading edges of traces D and E and the peak maximum does not shift between $\theta_{D2O} = 0.11$ and 0.18 ML. Apparently, the characteristics of zero-order desorption as shown in figure 4.2f only appear after a minimum coverage of water on the surface is exceeded.
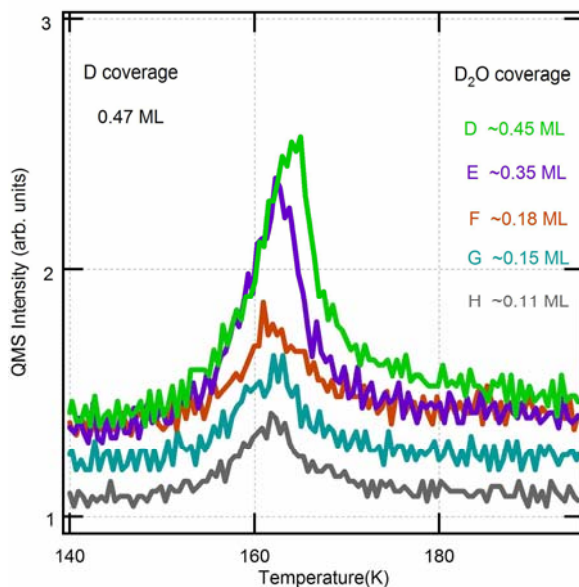

Figure 4.3 TPD of various amounts of D_2O deposited onto 0.47 ML D/Ni(111) at 85 K.

Using the simple decomposition scheme discussed in the experimental section, we have quantified the partitioning of water desorbing in the low and high temperature peaks. Figure 4.4 presents this partitioning for a fixed post-dose of ~1.0 ML D_2O in the range of $\theta_D = 0$ - 0.35 ML. With increasing θ_D, the fraction of D_2O molecules desorbing in the low temperature component increases at the expense of the fraction in the high temperature component. The shape of the curve shows two changes in slope near $\theta_D = 0.08$ ML and 0.3 ML creating three regions. For $\theta_D = 0$ - 0.08 ML, the slope for the high temperature partition equals ~2.5 ML D_2O/ML D. Between $\theta_D = 0.08$ and 0.30 ML it reduces to 0.3 ML D_2O/ML D. Beyond $\theta_D = 0.30$, the slope rapidly increases. Here, we can not determine a

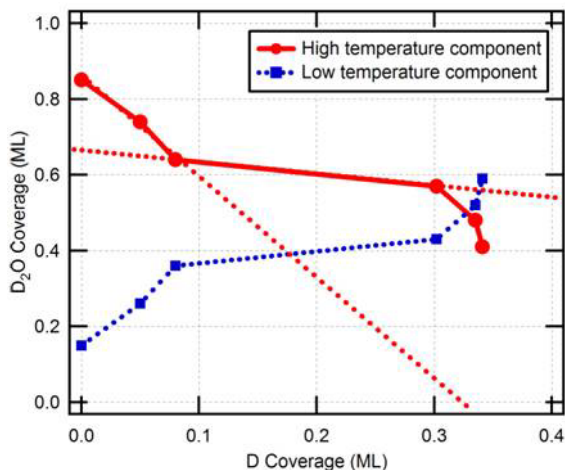slope since we can not decompose the high and low temperature features accurately beyond $\theta_D = 0.35$.

Figure 4.4 The partitioning of 1ML D_2O on various D pre-coverages on Ni(111).

In our previous study of $H_2O(D_2O)$/Ni(111) and D_2O/H/Ni(111) at Chapter 3, we have shown that HREEL spectra provide additional information regarding the bonding of water molecules adsorbed on Ni(111). In figure 4.5, we present such data for a $\theta_D = 0.3$ ML with varying θ_{D2O}. Figure 4.2e shows TPD spectra for the same deuterium pre-coverage where we noticed a deviation from water desorption behavior compared to lower D pre-coverages. For the bottom spectrum in figure 4.5, no D_2O was dosed. This spectrum was taken using an impact energy of the primary electron beam (E_p) of 9.6 eV with specular angle and shows a single feature at 90 meV. This feature is known to be caused by the Ni-D stretch vibration [23]. It is no longer observed when lowering E_p to 5 eV, as shown in the subsequent spectra in figure 4.5. This effect has been observed before for hydrogen adsorption on Ni(111) [33] and was attributed to resonance scattering [33,34]. Resonance scattering may be viewed as a special form of impact scattering. It involves transient formation of a negative ion and shows an energy-dependent scattering cross-section [35]. All other spectra shown in figure 4.5 were taken at $E_p = 5$ eV to ensure that observed energy losses in the same energy range cannot be attributed the to Ni-D stretch. The other three spectra shown in figure 4.5 for co-adsorption of D_2O and D all show the peak

attributed to the D-O-D bending vibration around 150 meV [2,30,36], and a broad feature between 50 and 100 meV generally attributed to D_2O librations [2,30,36]. We also observe the O-D stretch vibration at 310 meV. The intensity of the librations strongly increases with D_2O coverage. For $\theta_{D2O} = 0.90$ ML, the 28 meV peak attributed to D_2O-D_2O hydrogen-bonded translation normal to the (111) plane [2,30] is also clearly observable. In the 0.73 ML trace the same peak appears less pronounced as a shoulder on the elastic peak.
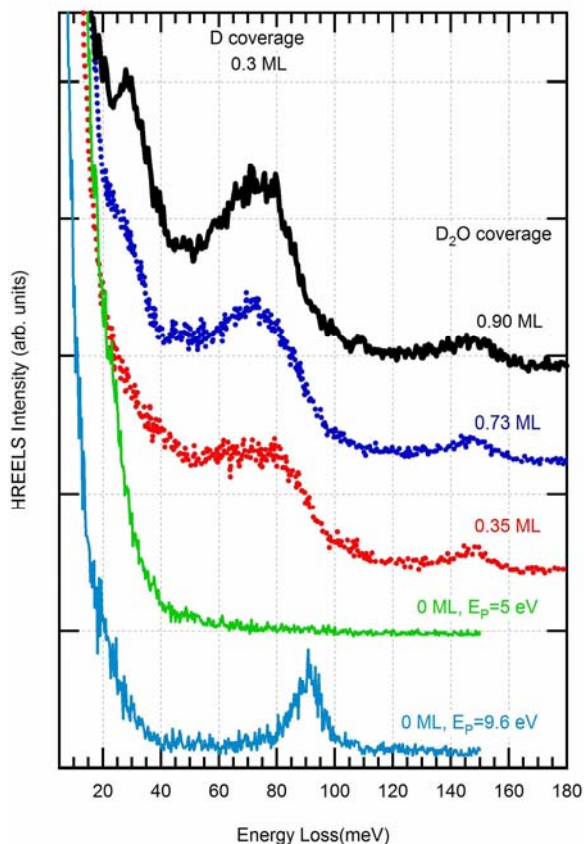

Figure 4.5 HREEL spectra of various D_2O coverages deposited onto 0.3 ML D/Ni(111).

Taking a different perspective, we have also investigated the influence of θ_D on desorption of a fixed post-coverage of 0.35 ML D_2O. Figure 4.6a plots TPD spectra of D_2O. We observe that the peak center shifts to lower temperatures with increasing θ_D. Figure

4.6b displays the center value of a Gaussian line shape fitted to the D_2O desorption traces from figure 4.6a as a function of θ_D. For this small D_2O post-coverage, the center value accurately matches the temperature at which the desorption rate is highest. For $0 < \theta_D < 0.3$ ML, the peak temperature shifts to lower values gradually at a rate of 2 K/ML D. Beyond $\theta_D = 0.3$ ML, the shift suddenly increases to ~25 K/ML D. Beyond $\theta_D = 0.50$ the shift of the peak center seems more gradual again and the slope is similar to the slope observed in the first section. The arrows in figure 4.6b point toward combinations of D and D_2O coverages for which also HREEL spectra were taken.
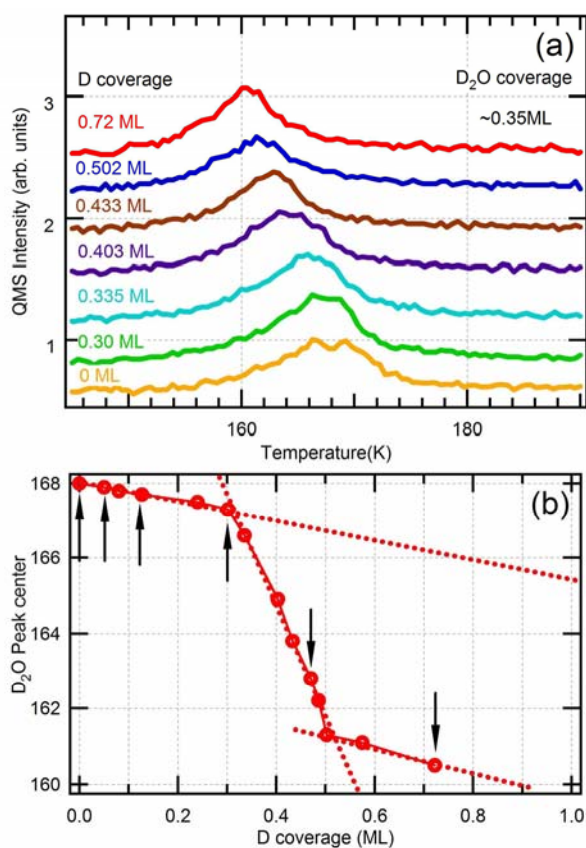

Figure 4.6 (a) TPD spectra of 0.35 ML D_2O on various D coverages. (b) D_2O peak center versus various D coverages.

Figure 4.7 shows the HREEL spectra corresponding to the D and D_2O coverages indicated in figure 4.6b by arrows. The HREEL spectrum for $\theta_D = 0$ ML shows an intense and relatively sharp feature at 80 meV. In addition, the background signal toward lower energy does not show the expected exponential decay from the elastic peak, indicating a very broad loss of low intensity centered near 50 meV. This broad loss develops into a distinct feature with increased D_2 dose and shifts up to ~75 meV at the highest coverage as shown here. The distinct peak at 80 meV does not shift and is still clearly observable in the HREEL spectra for $\theta_D = 0.05$ and 0.13 ML, although its intensity decreases relative to the upcoming feature at lower energy. The peaks merge completely for $\theta_D \geq 0.30$ ML. In relation to the TPD spectra for the same coverages in figure 4.6b, the loss of the distinct peak at 80 meV seems to coincide with the sharp turn at $\theta_D = 0.30$ ML in figure 4.6b. Only at the highest D coverage, we clearly observe the multilayer peak at 28 meV.
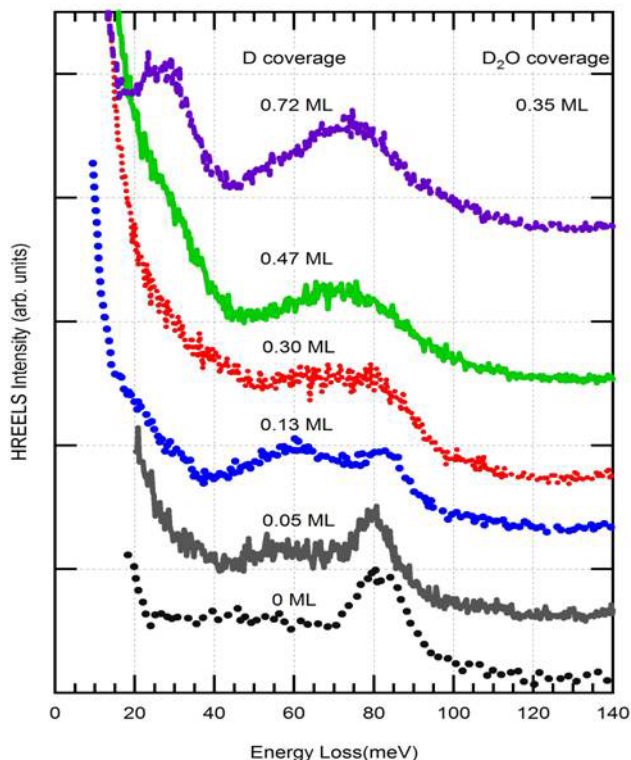

Figure 4.7 HREEL spectra of 0.35 ML D_2O deposited on various D coverages.

4.4 Discussion

First, we focus our attention on the TPD spectra in figure 4.2a. Our spectra are in excellent agreement with previously published spectra of water desorbing from bare Ni(111) [15-19]. It is generally agreed that the high temperature feature at ~170 K is attributed to the (sub)monolayer water desorption from the bare Ni(111) surface. The low temperature feature, starting at ~155 K, is ascribed to multilayer desorption. In our spectra, we observe that the high temperature feature shows zero-order desorption kinetics for lower coverages and first-order desorption kinetics at higher coverages. Observation of zero-order desorption kinetics is usually attributed to multilayer desorption, e.g. from multilayers of physisorbed noble gases or ice. Here, however, it is unlikely that water shows these characteristics at coverages far below 1 ML due to formation of multilayers. First, a separate desorption peak for multilayers 155 K has been identified [15-19]. Second, the 28 meV feature, which is indicative of multilayer formation [2,30,36], is absent [30]. To explain a similar observation for water desorption from Pt(111), Kay and co-workers recently suggested that water forms a two-phase system on the surface, consisting of a condensed phase and a 2-D gas-like phase, at thermodynamic equilibrium [37,38]. They argue that, under conditions present in their study, the rate of desorption is governed only by the temperature and thus zero-order kinetic behavior is observed. Since the same conditions also apply in our experiments, our TPD spectra for $\theta_D = 0$ and $\theta_{D2O} < 0.7$ ML can therefore be explained if water adsorbs as such a two-phase system onto the Ni(111) surface. The presence of at least the condensed phase on Ni(111) is in accordance with results from a previous RAIRS study that indicates formation of $(D_2O)_6$ clusters at both lower temperatures and much lower coverages [29].

Upward from $\theta_{D2O} = 0.7$ ML, desorption traces in figure 4.2a show first-order characteristics. Recent LEED experiments on water adsorption on Ni(111) show that a $(2\sqrt{7}x2\sqrt{7})R19°$ LEED pattern is observable after dosing more than 0.67 layer of water on Ni(111), although here water was adsorbed at 135 K [15]. Below 0.67 layer, absence of LEED patterns indicated that water did not have a tendency to form extended islands of any structure. Our observed change from zero-order to first order desorption kinetics then suggests that initial adsorption into co-existing condensed and gas-like phases has been

reduced to adsorption as a single phase at larger exposures. Summarizing, the results from these three combined studies suggest that, prior to desorption and up to ~ 0.7 ML, water forms a two-phase system consisting of a condensed phase of (extended) hexamer rings in equilibrium with a 2-D water gas. Beyond 0.7 ML, the entire system "freezes" into a single condensed phase with $(2\sqrt{7}x2\sqrt{7})R19°$ structure from which first-order desorption is observed.

Following this line of reasoning, enough bare nickel surface remains to accommodate the two-phase water system at low total coverages up until, at least, a deuterium pre-coverage of 0.13 ML. TPD traces in figure 2b, 2c, and 2d attest to this by the unchanged transition from zero-order to first-order desorption kinetics in the high temperature peak prior to the appearance of the low temperature peak around 155 K. It seems that the presence of such small amounts of deuterium mostly results in reducing available surface area for water adsorption without modifying the interaction of water with either the surface or itself significantly. Both experimental and theoretical studies have addressed how hydrogen adsorbs at such low coverages. A HREELS study suggests that the (2x2)-2H structure, which saturates the surface at $\theta_D = 0.5$ ML and which has also been observed with LEED [12], is likely also the dominant adsorption structure at much lower coverages and at a substrate temperature of 100 K [23]. Vibrational features of this structure remained visible down to $\theta_{D2O} = 0.05$ ML. Theoretical studies [21,39] support that this (2x2)-2H structure is more stable than the previously claimed p(2x2) structure [12], which could also exist in the range $0 < \theta_D < 0.25$ ML. Regardless, deuterium must obviously forms islands if it retains any of these structures at low coverages. With this in mind, it seems plausible that at the pre-coverages used in Figure 4.2b-2d, atomically-bound deuterium and water are not mixed on the surface but are adsorbed in separate islands. If they were mixed, the delicate balance between hydrogen bonding and the water-metal interaction [15] would be affected and result in measurable changes in TPD spectra. Therefore, we propose that water and atomically-bound hydrogen are phase segregated while both interact directly with the Ni(111) surface for these co-adsorption coverages. It may be that post-adsorption of water actually limits the mobility of atomic deuterium on the surface and enforces complete coalescence of a 2D atomic deuterium gas into deuterium islands.

If phase separation takes place, one may expect that it should be possible to use water as a titrant for the remaining bare nickel surface area after partial hydrogen adsorption. Indeed, this could provide a quantitative value for the hydrogen surface density at very low coverages, from which adsorption structures may be deducted or ruled out. A plot of the amount of water desorbing in the high temperature TPD feature as a function of deuterium pre-coverage, yields a slope that represents the area blocked for water adsorption by deuterium. If both axes are expressed in terms of their maximum coverage (here 1 ML), island formation of deuterium in a p(2x2) structure would yield a slope of 4, since at $\theta_D = 0.25$ ML the entire surface would be covered by this structure and no bare nickel surface remains for water adsorption. For a (2x2)-2D structure, it would result in a value of 2. Figure 4.4 is such a plot for a post-dose of ~1.0 ML D_2O. The upper trace represents the integrated area for water interacting with bare patches of the nickel surface as a function of D-coverage. The slope in the range $\theta_D = 0 - 0.1$ ML equals ~2.5, whereas it flattens to 0.3 up to $\theta_D = 0.3$ ML. Although the initial slope seems to agree reasonably well with a (2x2)-2D structure, we caution for qualifying this as strong evidence, since we have noticed partitioning between the low and high temperature peaks at $\theta_D = 0$. Partitioning here is likely a result of the experimental method and apparatus used to deposit water onto the surface. The interpolation in figure 4.4 may underestimate the slope at very low values of θ_D since the high temperature peak has not reached its maximum value for, at least, the data shown for $\theta_D = 0$ ML. Partitioning due to experimental procedures without being a consequence of hydrogen co-adsorption may also be present in data at slightly higher deuterium coverages. To check whether we can circumvent this complication, we have also performed the TPD decomposition for a wide range of θ_D using $\theta_{D2O} > 1.0$ ML with the more elaborate TPD fitting procedure mentioned in the experimental section. As mentioned before, results are more ambiguous at larger water coverages due to overlap of the TPD peaks, the required assumption of a particular analytical form to fit data, and the presence of pump tails. However, in all attempts to determine the slope using water as a titrant, we find values between 2 and 4 for $\theta_D < 0.1$ ML. Although these values are not inconsistent with hydrogen adsorbing in (mixed) islands of above mentioned structures, and perhaps

also without island formation, we do not feel that our analysis here is conclusive and attribute the scatter to the above mentioned assumptions in the TPD fitting procedure.

Returning to figure 4.4, we find another aspect noteworthy. In the range $0.1 < \theta_D < 0.3$ ML, the amount of water that desorbs in the high temperature peak diminishes only modestly. At $\theta_D = 0.3$ ML, we find $\theta_{D2O} = 0.6$ ML for the high temperature peak. This is significantly more (and beyond the uncertainty of our fitting procedure) than would fit onto the remaining bare surface if deuterium adsorbed as the more dense (2x2)-2D islands. We offer two possible explanations for this observation. First, growth of water islands may compress (2x2)-2D islands into partial (1x1)-D structures. Coexistence of the (2x2)-2D and (1x1)-1D structures has been observed for $0.5 < \theta_D < 1.0$ ML [12]. DFT calculations indicate that there is an energetic penalty for creation of (1x1)-1H from (2x2)-2H of 50 meV/H atom [21]. Energy differences between hydrogen-bonding and water-metal bonding for Ni(111) may be similar, although theoretical studies do not agree on the binding energy of a water molecule to the surface [27,28]. A recent LEED study suggests that energy differences between various structures that water may assume on the surface are likely small [15]. A second explanation for the almost unchanged partitioning in figure 4.4 for $0.1 < \theta_D < 0.3$ ML may be provided if water islands spill over onto hydrogen islands. The binding energy of such spill-over water molecules may only be diminished modestly in order for these to desorb as part of the high temperature TPD feature. This could be the case if the lateral hydrogen bonding is mostly retained.

The results shown in figure 4.6 can be interpreted to support either explanation. For a fixed amount of 0.35 ML D_2O, figure 4.6b shows that water desorption is not strongly affected by a deuterium pre-coverage up to approximately $\theta_D = 0.30$ ML. Beyond $\theta_D = 0.30$ ML, the rate of decline of the peak desorption temperature increases almost 10-fold. A second sharp turn in figure 4.6b occurs at $\theta_D = 0.5$ ML. Picking up the original idea that deuterium adsorbs as (2x2)-2D islands, it is logical that phase-separated hydrogen and water islands show no strong effects up to $\theta_D = 0.30$ ML, since, combined, they cover 95% of the surface. If deuterium remains adsorbed in this structure there is no bare nickel surface left at $\theta_D = 0.5$ ML. In the 'compression' scenario, the second inflection in figure 4.6b is then a result of not having any of the post-dosed water interacting with the bare

nickel surface to initiate compression of the deuterium layer. In the 'spill-over' scenario, an increasing fraction of the 0.35 ML post-dosed water is adsorbed by extending water islands over deuterium-covered regions.

However, when considering the size of the available patches of bare nickel surface left over when 0.3 ML deuterium adsorb as randomly distributed (2x2)-2D islands, it seems related to the size of hexamer ring structures, $(D_2O)_6$, which were deducted from RAIRS spectra [29]. The number of hydrogen bonds per water molecule is higher for ring structures (up to 1.5 per H_2O) than for linear chains (up to 1.0 per H_2O). A random distribution of (2x2)-2D islands at $\theta_D = 0.3$ ML leaves almost no bare nickel patches large enough to grow single ring structures and extensions from it, let alone for θ_D closer to 0.5. Therefore, we find that our observations are most easily explained if deuterium remains adsorbed mostly in a (2x2)-2D structure up to 0.5 ML with water molecules forming smaller and more disordered structures (e.g. short linear and branched chains) in between. The disordered water clusters are increasingly destabilized as a result of having fewer hydrogen bonds with increasing deuterium pre-coverage. This causes an increasingly lowered binding energy and lowered desorption temperature.

Two different observations suggest that water does not initially form a multilayered structure when a larger amount of water is dosed than which 'fits' into the empty nickel surface area in the range $0.1 < \theta_D < 0.3$ ML. First, the 155 K feature known to represent multilayer formation of water in TPD spectra does not appear in figure 4.6a as it does in figure 4.2b-2e. Instead we see a gradual shift to lower desorption temperatures, indicative of a gradual change in binding energy. Second, we do not observe the 28 meV feature indicative of multilayer formation in figure 4.7 up to $\theta_D > 0.5$ ML. The peak just appears as a shoulder on the elastic peak for $\theta_{D2O} = 0.35$ ML with $\theta_D = 0.47$ ML. Therefore, some spill-over seems to occur prior to formation of a multilayer in this regime.

With this description of water adsorption at the metal interface with deuterium pre-coverage ranging from 0 to 0.3 ML, we can now revisit the TPD features observed in figure 4.2b-2e. For low total coverages, separate deuterium and water islands are formed. When the remaining bare nickel surface area is large enough, water assumes a two-phase system at equilibrium. With increasing water dose, a point is reached where the additional water

cannot be accommodated on the bare metal surface. Depending on the size of the deuterium islands, water either adsorbs as a multilayer or spills over onto deuterium islands. The shapes and shifts of traces in figure 4.2e (and to some extent in 2d) suggest that spill over is also followed by growth of a (disordered) multilayer for higher doses. The two HREEL spectra for the larger total coverages in figure 4.5 confirm this suggestion through the appearance of the 28 meV feature.

Having discussed water adsorption on lower pre-coverages, we turn to deuterium pre-coverages of ~0.5 ML and higher. Figure 4.2f and 4.3 suggest that initially a small amount of water adsorb as water clusters onto a (mostly) saturated (2x2)-2D structure. These clusters grow laterally up to ~0.2 ML before acting as nucleation sites for 3D growth of disordered 'snowballs' that show approximate zero-order desorption kinetics. The increase in surface area with increasing radius of such, roughly, hemispherical structures would, at least qualitatively, result in the deviation of zero-order desorption kinetics as observed in figure 4.2f. The observed sudden changes in the leading edges may even suggest layer-by-layer growth of such 3D structures. Beyond $\theta_D > 0.5$ ML the peak desorption temperature (figure 4.6b) continues to drop slowly indicating that mixed (1x1)-1D and (2x2)-2D structures are also hydrophobic. When extrapolated to $\theta_D = 1.0$ ML we obtain from figure 4.6b the same desorption temperature as expected for 0.35 ML D_2O from our previous study in Chapter 3. Also, the typical 28 meV feature in HREEL spectra appears at very low water coverages as shown in the top trace in figure 4.7. A rough estimate based on relative intensities of HREEL features for the librations and the D_2O-D_2O normal translation suggests that for $\theta_D = 0.72$ ML and $\theta_{D2O} = 0.35$ ML, the hemispherical 'snowballs' are similar in thickness as the flatter structure created at $\theta_D = 0.30$ ML and $\theta_{D2O} = 0.90$ ML.

In Chapter 3 we attributed the 80 meV peak in D_2O HREEL spectra, as shown in figure 4.7, to the rocking motion of water molecules. We had found this feature to result from dipole scattering and suggested that this mode could be characteristic of the $(2\sqrt{7}x2\sqrt{7})R19°$ structure. The other libration feature around 50 meV was attributed to the wag and twist motions of water molecules. However in figure 4.7, for $\theta_{D2O} = 0.35$ ML and $\theta_D = 0.13$ ML the 80 meV peak is still clearly observable, whereas in such case the formation of the 'frozen' $(2\sqrt{7}x2\sqrt{7})R19°$ structure is not yet expected. Our data actually show that, with

increasing θ_D, the relative intensity of this peak decreases while the relative intensity of the wag and twist feature increases. This seems at odds with a description that attributes these features to a single species on the surface. As we discussed earlier, with increasing θ_D, we expect the mobility of free water molecules (2D gas) to be reduced up to a point where the entire system freezes. With the same increase, the relative number of free gas-like water molecules is decreased compared to the number in the condensed phase. At $\theta_D = 0.30$ ML, the whole system seems frozen, and almost no free gas-like molecules are left. These considerations lead us to speculate that the 80 meV peak is actually related to librations of water molecules in a 2D gas, whereas the 50-75 meV peak results from librations in the condensed phase. We are aware of only one theoretical study that has addressed vibrational frequencies for single H_2O molecules on Ni(111). This study has predicted that the H_2O-Ni stretch, which may be expected to show strong dipole scattering, appears at 75 meV [28], in reasonable agreement with the strong loss observed at 80 meV.

Finally, we compare our results obtained for co-adsorption of D and D_2O on Ni(111) to similar data for Pt(111). For the latter, the most recent and detailed desorption spectra [9] indicates that post-dosing 2 ML D_2O on top of varying pre-doses of D initially results in stabilization of the water layer closest to the metal. Petrik and Kimmel show that, up to a D-atom density of 3.5×10^{14} cm^{-2} (which corresponds to ~0.25 ML when assuming a 1.0 ML D/Pt saturation coverage) a separate desorption peak with a maximum desorption temperature of ~5 K higher than the monolayer desorption peak, appears in TPD spectra. The new, higher temperature peak grows in at the expense of the original peak. At pre-coverages exceeding $\theta_D = 3.5 \times 10^{14}$ cm^{-2}, the D_2O desorption peak shifts back to lower temperatures (to ~170 K) and reduces in size. We distinguish two main differences between the effect of hydrogen pre-adsorption on water adsorption for Pt(111) and Ni(111). First, stabilization of water by atomic deuterium does not occur on Ni(111). On Pt(111), stabilization may be related to formation of H_3O^+ species [3]. No evidence was found for formation of such species on Ni(111) by TPD and HREELS as we discussed in Chapter 3. Second, at very large deuterium doses, water desorption from Pt(111) shows no reduction in binding energy of D_2O compared to the bare surface. On Ni(111), the drop in desorption temperature for small amounts of water adsorbed on a hydrogen overlayer reaches ~10 K.

Apparently, conversion of bare Ni(111) to H-covered Ni(111) makes the surface considerably more hydrophobic, whereas it does not on Pt(111).

The difference in the observed sign of the work function change upon dissociatively adsorbing hydrogen on these surfaces provides a possible explanation for this difference. On Pt(111), the work function decreases by 230 mV by adsorption of ~0.8 ML of the saturation coverage of hydrogen [40,41]. On Ni(111) a work function increase of 195 meV was observed upon adsorbing hydrogen [11]. The difference in hydrophobic character may therefore be a result of repelling (Ni) or attracting (Pt) local fields between D_2O_{ads} and D_{ads}.

A second explanation for the difference between the effect of hydrogen adsorption at large doses may be provided by analogy to the observed hydrophobic character of a monolayer of crystalline ice on Pt(111) grown at substrate temperatures above 135 K [38]. Here, hydrophobicity was argued to result from a lack of dangling OH bonds and lone pairs to interact with a second layer of water molecules. Water molecules in the first layer had previously been shown to bond alternatively through an oxygen lone pair and a hydrogen atom [42]. If a water (sub)monolayer grown at 85 K on Ni(111) also orders itself using Ni-HO bonds, pre-adsorption of hydrogen likely makes this type of bonding unfavorable, enforcing a different bonding structure. Experiments using rare gas [38], chloroform [43], or bromoform [44] adsorption may assist in judging whether the first layer of water on Ni(111) resembles the first crystalline ice layer grown on Pt(111).

4.5 Summary

Figure 4.8 summarizes our results regarding water adsorption onto a partially deuterium-covered Ni(111) surface. For $0 < \theta_D < 0.1$ ML and low θ_{D2O}, deuterium and water segregate into islands. Our data does not provide information on possible adsorption structures of D atoms, but strongly suggests that D_2O forms a two-phase system at equilibrium. We propose that it consists of a condensed phase, likely based on a hexamer ring structure ("hex", red), and a 2D gas phase (marked by single D_2O molecules, although this may not be the dominant species in that phase). This two-phase system is characterized by zero-order desorption kinetics and a distinct 80 meV feature in HREEL spectra. The latter may be related to the 2D gas phase. For $0 < \theta_D < 0.1$ ML and high θ_{D2O}, deuterium and water

islands are still phase segregated. D_2O has 'frozen' into a single phase prior to formation of a multilayer ("ML", purple). The multilayer gives rise to the 155 K desorption feature and a 28 meV loss in HREEL spectra. For $0.1 < \theta_D < 0.3$ ML, D atoms are most likely forming (2x2)-2D islands. At low θ_{D2O}, water and deuterium still phase segregate and D_2O forms the two-phase system as described before. For higher θ_{D2O}, additional D_2O spills over onto D-islands forming more disordered structures ("dis", orange) and/or multilayers. Spill-over versus multilayer formation is governed by the size of water and deuterium islands. In this range, desorption spectra show less discriminate increases in the high and low temperatures features. For $0.3 < \theta_D < 0.5$ ML, we suggest that water can no longer form hexagonally-based structures in direct contact with the nickel surface and that smaller water clusters in between deuterium islands form nucleation sites for growth of disordered 3D structures. For $\theta_D > 0.5$ ML, D_2O molecules initially cluster on a mixed (1x1)-1D / (2x2)-2D surface before growing 3D structures. The underlying deuterium layer is increasingly hydrophobic upon approaching saturation.
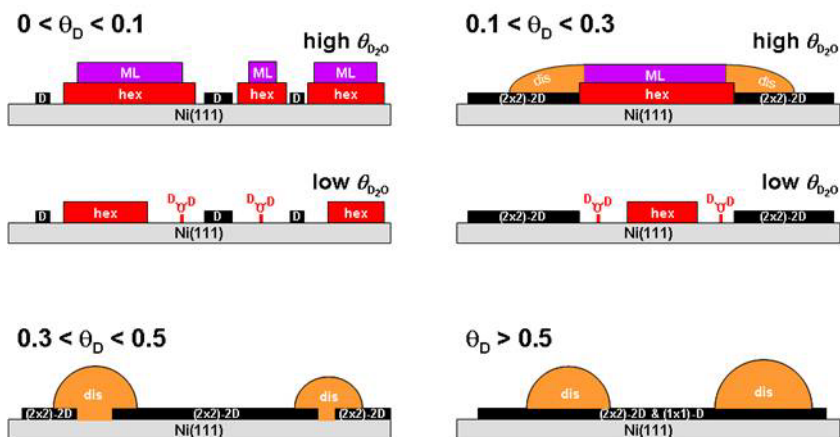

Figure 4.8 Schematic representations of adsorbed structures for water and deuterium. See text for details on color coding and abbreviations.

4.6 References

[1] M. A. Henderson, *Surf. Sci. Rep.*, 2002, **46**, 5.

[2] K. Jacobi, K. Bedurftig, Y. Wang, and G. Ertl, *Surf. Sci.*, 2001, **472**, 9.

[3] F. T. Wagner, and T. E. Moylan, *Surf. Sci.*, 1988, **206**, 187.

[4] S. K. Jo, J. A. Polanco, and J. M. White, *Surf. Sci.*, 1988, **253**, 233.

[5] G. B. Fisher, and J. L. Gland, *Surf. Sci.*, 1980, **94**, 446.

[6] J. Schott, D. Lackey, and J. K. Sass, *Surf. Sci.*, 1990, **238**, L478.

[7] N. Chen, P. Blowers, and R. I. Masel, *Surf. Sci.*, 1999, **419**, 150.

[8] N. Kizhakevariam, and E. M. Stuve, *Surf. Sci.*, 1992, **275**, 223.

[9] N. G. Petrik, and G. A. Kimmel, *J. Chem. Phys.*, 2004, **121**, 3727.

[10] C. D. Taylor, R. G. Kelly, and M. Neurock, *J. Electrochem. Soc.*, 2007, **154**, F55.

[11] K. Christmann, O. Schober, G. Ertl, and M. Neumann, *J. Chem. Phys.*, 1974, **60**, 4528.

[12] K. Christmann, R. J. Behm, G. Ertl, M. A. Van Hove, and W. H. Weinberg, *J. Chem. Phys.*, 1979, **70**, 4168.

[13] A. Winkler, and K. D. Rendulic, *Surf. Sci.*, 1982, **118**, 19.

[14] K. Mortensen, F. Besenbacher, I. Stensgaard, and W. R. Wampler, *Surf. Sci.*, 1988, **205**, 433.

[15] M. E. Gallagher, S. Haq, A. Omer, and A. Hodgson, *Surf. Sci.*, 2007, **601**, 268.

[16] T. E. Madey, and F. P. Netzer,, *Surf. Sci.*, 1982, **117**, 549.

[17] R. H. Stulen, and P. A. Thiel, *Surf. Sci.*, 1985, **157**, 99.

[18] T. Pache, H. P. Steinruck, W. Huber, and D. Menzel, *Surf. Sci.*, 1989, **224**, 195.

[19] C. Mundt, and C. Benndorf, *Surf. Sci.*, 1993, **287/288**, 119.

[20] B. Bhatia, and D. S. Sholl, *J. Chem. Phys.*, 2005, **122**, 204707.

[21] J. Greeley, and M. Mavrikakis, *Surf. Sci.*, 2003, **540**, 215.

[22] R. Baer, Y. Zeiri, and R. Kosloff, *Phys. Rev. B*, 1997, **55**, 10952.

[23] H. Yanagita, J. Sakai, T. Aruga, N. Takagi, and M. Nishijima, *Phys. Rev. B*, 1997, **56**, 14952.

[24] A. C. Luntz, J. K. Brown, and M. D. Williams, J. Chem. Phys., 1990, **93**, 5240.

[25] K. Christmann, *Surf. Sci. Rep.*, 1988, **9**, 1.

[26] G. X. Cao, E. Nabighian, and X. D. Zhu, *Phys. Rev. lett.*, 1997, **79**, 3696.

[27] M. Pozzo, G. Carlini, R. Rosei, and D. Alfè, *J. Chem. Phys.*, 2007, **126**, 164706.

[28] H. Yang, and J. L. Whitten, *Surf. Sci.*, 1989, **223**, 131.

[29] M. Nakamura, and M. Ito, *Chem. Phys. Lett.*, 2004, **384**, 256.

[30] J. Shan, J. F. M. Aarts, A. W. Kleyn, and L. B. F. Juurlink, *Phys. Chem. Chem. Phys.*, 2008, **10**, 2227; this thesis chapter 3.

[31] C. T. Campbell, and S. M. Valone, *J. Vac. Sci. Technol. A.*, 1985, **3**, 408.

[32] A. M. Dejong, and J. W. Niemantsverdriet, *Surf. Sci.*, 1990, **233**, 355.

[33] A. D. Johnson, K. J. Maynard, S. P. Daley, Q. Y. Yang, and S. T. Ceyer, *Phys. Rev. lett.*, 1991, **67**, 927.

[34] H. Ibach, and D. L. Mills, *Electron Energy Loss Spectroscopy and surface Vibrations*, Academic Press, New York, 1982.

[35] G. J. Schulz, *Rev. Mod. Phys.*, 1973, **45**, 423.

[36] B.A. Sexton, *Surf. Sci.*, 1980, **94**, 435.

[37] J. L. Daschbach, B. M. Peden, R. S. Smith, and B. D. Kay, *J. Chem. Phys.*, 2004, **120**, 1516.

[38] G. A. Kimmel, N. G. Petrik, Z. Dohnalek, and B. D. Kay, *Phys. Rev. Lett.*, 2005, **95**, 166102.

[39] G. Kresse, and J. Hafner, *Surf. Sci.*, 2000, **459**, 287.

[40] K. Christmann, G. Ertl, and T.Pignet, *Surf. Sci.*, 1976, **54**, 365.

[41] K. Christmann, and G. Ertl, *Surf. Sci.*, 1976, **60**, 365.

[42] H. Ogasawara, B. Brenda, D. Nordlund, M. Nyberg, A. Permenschikov, L. G. M. Pettersson, and A. Nilsson, *Phys. Rev. Lett.*, 2002, **89**, 276102.

[43] G. Zimbitas, and A. Hodgson, *Chem. Phys. Lett.*, 2006, **417**, 1.

[44] M. L. Grecea, E. H. G. Backus, H. J. Fraser, T. Pradeep, A. W. Kleyn, and M., Bonn, *Chem. Phys. Lett.*, 2004, **385**, 244.

Chapter four